4 Glacial Isostatic Adjustment and Relative Sea-Level Change

W. RICHARD PELTIER
University of Toronto

ABSTRACT

Secular trends of relative sea level revealed on tide-gauge records have recently been interpreted as requiring some eustatic increase of sea level to have occurred during the past century. Although allowance in interpreting these data is usually made for a contribution due to thermal expansion of ocean volume, it is not generally recognized that the continuing influence of glacial isostatic disequilibrium also contributes significantly to the observed secular trends. The eastern seaboard of the continental United States is a geographical region in which this source of "contamination" is especially large. This fact is discussed in illustration of a global model of deglaciation-induced relative sea-level change, which may be employed to filter the isostatic signal from the tide-gauge data. The same geophysical model has also been successfully employed to explain certain anomalies of the Earth's rotation that have been previously invoked to support the notion that a eustatic increase of sea level must be occurring at present. The anomalies consist of the ongoing wander of the rotation pole toward Hudson Bay at a rate near 1° per million years, and the so-called nontidal component of the Earth's acceleration of rotation that has recently been observed with the LAGEOS satellite. Both anomalies are explicable as memories of the most recent deglaciation event of the current ice age.

INTRODUCTION

The purpose of this chapter is to review results of research conducted over the past decade concerning the nature of relative sea-level (RSL) variations forced by disintegration of the huge continental ice sheets that covered Canada, Northwestern Europe, and West Antarctica at Würm-Wisconsin maximum 18,000 years ago (18 ka). The melting of these ice sheets was essentially complete by 7 ka and resulted in a net rise of mean sea level over the global ocean of about 130 m. The rate of eustatic rise during the glacial-interglacial transition was therefore approximately 10 mm/yr. In spite of the fact that melting has been complete for so many millennia, RSL continues to vary in response to this cause due to the extremely high value of the effective viscosity of the planetary mantle that governs the rate of return to isostatic (gravitational) equilibrium. To fix orders of magnitude it is useful to recall that pres-

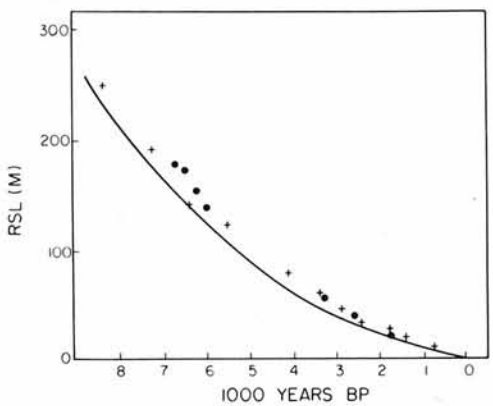

FIGURE 4.1 (a) This photograph shows a flight of raised beaches that are located in the Richmond Gulf on the southeast shore of Hudson Bay near the center of postglacial rebound. (b) The relative sea-level (RSL) curve from the Richmond Gulf beaches shown in (a). The age of individual horizons is determined by ^{14}C dating of relict beach material.

ent-day rates of RSL fall in the three regions that were previously ice covered are approximately 1 cm/yr. The main observational data that have been employed to demonstrate this fact consist of ^{14}C-controlled RSL histories in the age range 0 to 12 ka. These data are obtained from flights of raised beaches such as those shown in Figure 4.1a, which are located in the Richmond Gulf on the southeast shore of Hudson Bay near the center of postglacial rebound. Individual relict beaches in the sequence may be dated using the radiocarbon method and their heights above present-day sea level plotted as a function of their age to obtain a local history of relative sea level such as that shown in Figure 4.1b for the Richmond Gulf sequence. Such data make up the primary geophysical database for the inference of mantle viscosity, a physical parameter that is fundamental to the understanding of continental

drift and many other geodynamic processes. A recent review of solid-earth geophysical applications of RSL data is provided in Peltier (1982).

Although radiocarbon data on raised beaches, such as those shown in Figure 4.1, demonstrate that the surface of the solid earth has been rising monotonically with respect to the geoid since glaciation was complete at sites that were once ice covered, the opposite sense of RSL variation has persisted in the regions immediately peripheral to the margins of the major ice sheets. That this should be the case is simply understandable on the basis of the principle of conservation of mass. At glacial maximum, the Earth is depressed under the weight of the ice, approximately by the amount required for the buoyant restoring force due to the surface deflection (the Archimedes force) to balance the weight of the load. The material that must be removed from beneath the ice sheet to accommodate the sinking of the Earth flows viscously into the immediately peripheral region where the land is elevated. This region will subsequently be referred to as the peripheral bulge. When the ice sheet disintegrates, this process reverses and the land rises with respect to sea level in places that were once ice covered, and beaches such as those shown on Figure 4.1 are cut into the land where it contacts the sea, thus constituting a history of the recovery process. In the peripheral region, however, the land sinks with respect to sea level and relict beaches are drowned. An excellent example of a drowned coast produced by glacial peripheral bulge collapse is provided by the east coast of the continental United States, all of which is peripheral to the huge Laurentide ice mass that covered Canada 18 ka. An illustrative set of ^{14}C-controlled RSL data from sites along this coast is shown in Figure 4.2. Inspection of these

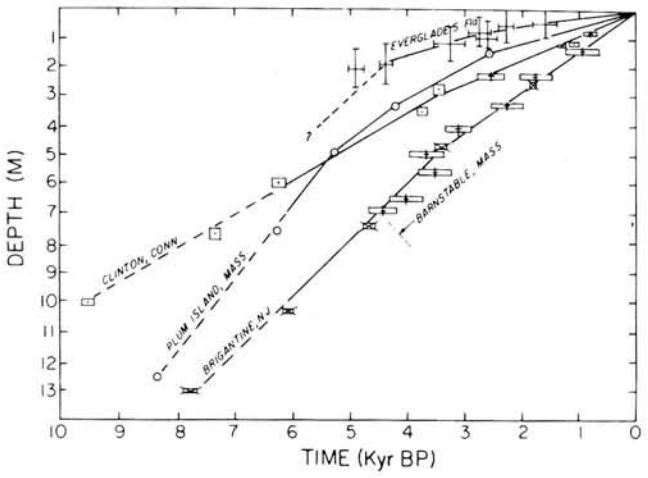

FIGURE 4.2 Relative sea-level data from a number of sites along the east coast of the United States. Adapted from Bloom (1967).

data demonstrates that the rate of sea-level rise at some sites along the coast (e.g., Barnstable, Massachusetts) is in excess of 1 mm/yr. Although this rate is an order of magnitude less than the rate of sea-level fall that obtains within the central Laurentide depression, it is nevertheless a rate that is rather significant from several points of view.

Most important for our purposes is the fact that this rate of RSL rise is close to that which has been inferred on the basis of tide-gauge observations of secular sea-level trends and interpreted in terms of implications for climate change (e.g., Hansen *et al.*, 1981). Recent analyses of these data (reviewed by Barnett, Chapter 1, this volume) reinforce the conclusions of earlier workers to the effect that on a global basis the data suggest that RSL is currently rising at a rate of 1 to 2 mm/yr. Gornitz *et al.* (1982), for example, concluded that the tide-gauge data imply a global increase of RSL at a rate near 1 mm/yr. The most straightforward interpretation of this observation, assuming that the claim made for its global validity is justified, is that the volume of water in the global ocean is currently increasing. Although this could, in principle, be caused by thermal expansion of the water column (a process discussed in detail by Roemmich, Chapter 13, this volume), the estimate by Gornitz *et al.* (1982) of the possible contribution owing to this effect suggests that it is able to explain no more than 50 percent of the observed rate of RSL rise. If this is a valid upper bound, it implies that the mass of water in the oceans must also be increasing and, therefore, that water "normally" stored in continental ice complexes is being returned to the oceanic reservoir, this being the only conceivable source for the amounts of water required to balance the observation. Hansen *et al.* (1981) suggested that this implied wastage of continental ice masses could be the first indication of the global climate amelioration that is expected as a result of the increasing atmospheric concentrations of carbon dioxide and other "greenhouse" gases. Meier (1984) recently discussed the compatibility of this hypothesis of a current retreat of continental ice with the available glaciological evidence. His conclusion (also discussed in Chapter 10, this volume) is that although there is no evidence supporting the possibility of a significant ongoing reduction of either Greenland or Antarctic ice, there is strong evidence to the effect that a reduction in volume of the small ice sheets and glaciers of the world is occurring, which could very well provide the mass required to balance the RSL analyses of Gornitz *et al.* (1982).

The possible climatological implications of the secular variation of RSL, discussed above, that has been extracted from the tide-gauge data, are clearly important. They do hinge crucially, however, on the assumption that the secular trend of 1 to 2 mm/yr is a number that is globally representative. Unfortunately, and as discussed at length by Barnett (Chapter 1, this volume), the existing network

of tide gauges does not provide uniform coverage over the globe so that a severe sampling problem exists. Furthermore, many of the most heavily instrumented coastlines of the world, such as the west coast of the North American continent and coastal Japan, are strongly influenced by local tectonic processes and, therefore, are unlikely to provide any reliable information on eustatic water rise. At these locations, the vertical motions of the solid earth associated with the dominantly strike-slip earthquakes that mark the San Andreas Fault and the dip-slip earthquakes associated with active subduction in the Japan trench are expected to obscure the eustatic signal. Other heavily instrumented coastlines such as the passive continental margins of the east coast of North America and northwestern Europe might be considered more likely regions to provide a signal that is free of such tectonic contamination. These coastlines are however located, respectively, on the forebulges of the ancient Laurentian and Fennoscandian ice sheets so that, as discussed above, sea level in these regions will appear to be rising as a consequence of the sinking of the land with respect to the geoid that accompanies the isostatic readjustment of the surface following deglaciation. If it were possible to correct these passive margin data for the influence of glacial isostatic disequilibrium, the residual trends so obtained might be particularly useful as constraints on the current rate of eustatic water rise (fall) cause by steric and ice-sheet disintegration effects.

Over the past decade a geophysical model has been developed that is ideally suited to the task of filtering from the RSL record, at any tide-gauge station on the Earth's surface, the contribution to the secular change of RSL resulting from current glacial isostatic disequilibrium. This model is based on the mathematical analysis of the deformation of a viscoelastic Earth produced by surface mass loads originally presented in Peltier (1974). It was first employed by Peltier and Andrews (1976) to predict variations of RSL forced by Pleistocene deglaciation; their calculations were based on the assumption that the water produced by ice-sheet melting could be assumed to be distributed uniformly over the ocean basins. Farrell and Clark (1976) showed how this mathematical analysis could be extended to determine the way in which the meltwater must be distributed within and among the ocean basins such that the instantaneous geoid remained an equipotential surface at all times during and subsequent to the ice-sheet disintegration event. The first predictions of expected RSL variations with the complete theory were described in Clark *et al.* (1978) and Peltier *et al.* (1978). By comparing these predictions with ^{14}C-controlled RSL observations such as those illustrated in Figure 4.1, it was demonstrated that a large fraction of the variance in the global RSL record over the age range 0 to 18 ka could be explained. In particular the previously enigmatic observation of raised beaches at sites in the southern ocean at times subsequent to 6 ka (e.g., Russell, 1961) was shown to be a natural consequence of the global-scale viscoelastic adjustment process following a deglaciation that ended about 7 ka.

Although one other global model of RSL change has also been produced (Cathles, 1975), it suffers from two crucial flaws. First, it is not gravitationally self-consistent and so does not accurately predict far-field RSL data; second, it does not incorporate a surface lithosphere and so cannot accurately predict RSL data in the near field. All of the discussion to be presented here will therefore be based on the more accurate model.

In the past few years several additional geophysical observations have been shown to be explicable in terms of extensions of the same theory developed in the papers cited above to explain deglaciation-induced RSL change. The large-scale negative free-air gravity anomalies observed over the three main centers of postglacial rebound have been shown to be compatible with the same viscoelastic model that fits the RSL data (Peltier, 1980, 1981; Peltier and Wu, 1982; Wu and Peltier, 1983). Also, the large misfits between predicted and observed RSL data (Peltier *et al.*, 1978; Clark *et al.*, 1978) at sites in the peripheral bulge regions have been shown to be due to the neglect of the influence of the surface lithosphere (Peltier, 1984b). Finally, two rather important and previously unexplained anomalies in the Earth's rotation, namely, the true wander of the rotation pole toward Hudson Bay at a rate near $1°/10^6$ yr, which is revealed in the International Latitude Service path, and the so-called nontidal component of the acceleration of the axial rate of rotation, which has recently been observed using the LAGEOS satellite, have also been shown to be consistent with the same viscoelastic Earth structure (Sabadini and Peltier, 1981; Peltier, 1982, 1983, 1984a, 1985a; Peltier and Wu, 1983; Wu and Peltier, 1984). That the latter effect might be due to glacial isostatic adjustment was first suggested by Dicke (1969), who suggested that it could be employed to constrain mantle viscosity—a notion that was later investigated in more quantitative fashion by O'Connell (1971). The former observation is particularly important as it was originally invoked by Munk and Revelle (1952) in support of the notion that some current retreat of the Earth's major ice sheets must be occurring to account for it. Their argument has been resurrected in the recent literature on the secular variation of RSL seen on tide gauges, in support of the same idea (e.g., Barnett, 1983). The analysis first reported in Peltier (1982) demonstrated that the theoretical argument employed by Munk and Revelle is incorrect, however. When the radial variations of viscoelastic structure of the real Earth are properly taken into account,

it is shown that the observed polar wander toward Hudson Bay can be explained entirely as an ongoing effect due to the deglaciation event that ended about 7 ka. No current wastage of continental ice is therefore required to understand this observation, and the data may in fact be construed as arguing against this possibility.

The remainder of this chapter provides a more detailed discussion of the evidence cited above to the effect that this viscoelastic model does in fact fit the wide range of geophysical data. Since the model does fit, in particular, the observed RSL record in the age range 0 to 18 ka rather well, it may reasonably be employed to predict the present-day rate of RSL variation that should be occurring at any site at which a tide gauge is located. This is the secular change that a tide gauge should record if glacial isostatic disequilibrium were the only source of RSL change at the site in question. The viscoelastic model is then employed to predict the present-day rate of vertical motion with respect to the geoid of the surface of the land everywhere on the North American continent. A map of this field is presented. This demonstrates that present-day rates of RSL rise along the U.S. east coast caused by glacial isostatic disequilibrium may be as high as 2 mm/yr. The field theory is then employed to filter this effect from the secular trends observed on all tide gauges located along both the east and west coasts of the continental United States. The average of the residual trends at U.S. East Coast sites is still significantly different from zero and has a value near 1 mm/yr. However, variations about the mean are extreme on rather small spatial scales and indicate contributions to the residual from sources other than eustatic water rise. In conclusion, a brief summary and discussion of future prospects for further applications of the isostatic adjustment model of RSL change reviewed here is presented.

THE GLOBAL MODEL OF GLACIAL ISOSTASY

The mathematical structure of the global model of glacial isostatic adjustment has been reviewed in Peltier (1982), to which the interested reader is referred for details and for a much more complete review of the history of this subject than could be presented here. In this model the planetary interior is assumed to be radially stratified with an elastic structure fixed by observations of the frequencies of the elastic gravitational normal modes of free oscillation as described, for example, by Gilbert and Dziewonski (1975). The rheology of the interior is assumed to be linearly viscoelastic and of the "Maxwell" type, in which the initial response to an applied shear stress is Hookean elastic, but the final response is Newtonian viscous. The depth-dependent viscosity in the model is therefore the only parameter that one can vary in order to fit RSL data, such as those shown in Figure 4.1. In the actual prediction of such RSL variations, one assumes a melting history for all of the surface ice loads that exist at glacial maximum and then computes, in a gravitationally self-consistent fashion, the manner in which the meltwater must be distributed over the global ocean in order to ensure that the instantaneous surface of the new ocean is maintained as an equipotential surface at all times. This operation requires inversion of an integral equation at every instant during and subsequent to the deglaciation, and results in a direct prediction of the time-dependent separation of the geoid and the surface of the solid earth at any point on the Earth's surface where ocean and land meet. In the model the geography of oceans and continents is realistically described and the full effects of gravitation are accounted for including the gravitational attraction of the water by the ice and the self-attraction of the water. The integral equation is inverted using a finite-element discretization of the surface, and a Green's function formalism is employed to describe the gravitational interactions between the aquasphere, cryosphere, and solid-earth components of the model that are fundamental to the determination of sea-level change. It is important to be able to make a reasonably accurate *a priori* estimate of the deglaciation history subsequent to 18 ka since we would not otherwise be in a good position to invert the predictions of the model to recover the radial variation of mantle viscosity. Peltier and Andrews (1976) described the way in which ^{14}C-age-controlled terminal moraine data can be combined with far-field observations of RSL and ice-mechanical considerations to develop first-order models of the glacial chronology. Their initial model, called ICE-1, has since been improved by Wu and Peltier (1983), who have called the new model ICE-2. This model is illustrated in Figure 4.3. The forward problem for RSL prediction takes as input this glaciation history and a model of the planet's radial viscoelastic structure and produces as output a prediction of the RSL variation that should be observed at any site of interest. These predictions are illustrated in the following subsections.

Postglacial Variations of Relative Sea Level

Typical examples of observed and predicted RSL variations at a number of sites on the North American continent are illustrated on Figure 4.4 for six locations, three at sites that were once ice covered (a, b, and c) and three for sites along the east coast of the continental United States in the peripheral region of monotonic subsidence (d, e, and f). The Earth model employed to make these predictions has elastic structure 1066B of Gilbert and Dziewonski (1975), an upper mantle viscosity of 10^{21} Pa s, and a lower mantle viscosity beneath 670 km of 2×10^{21} Pa s. On

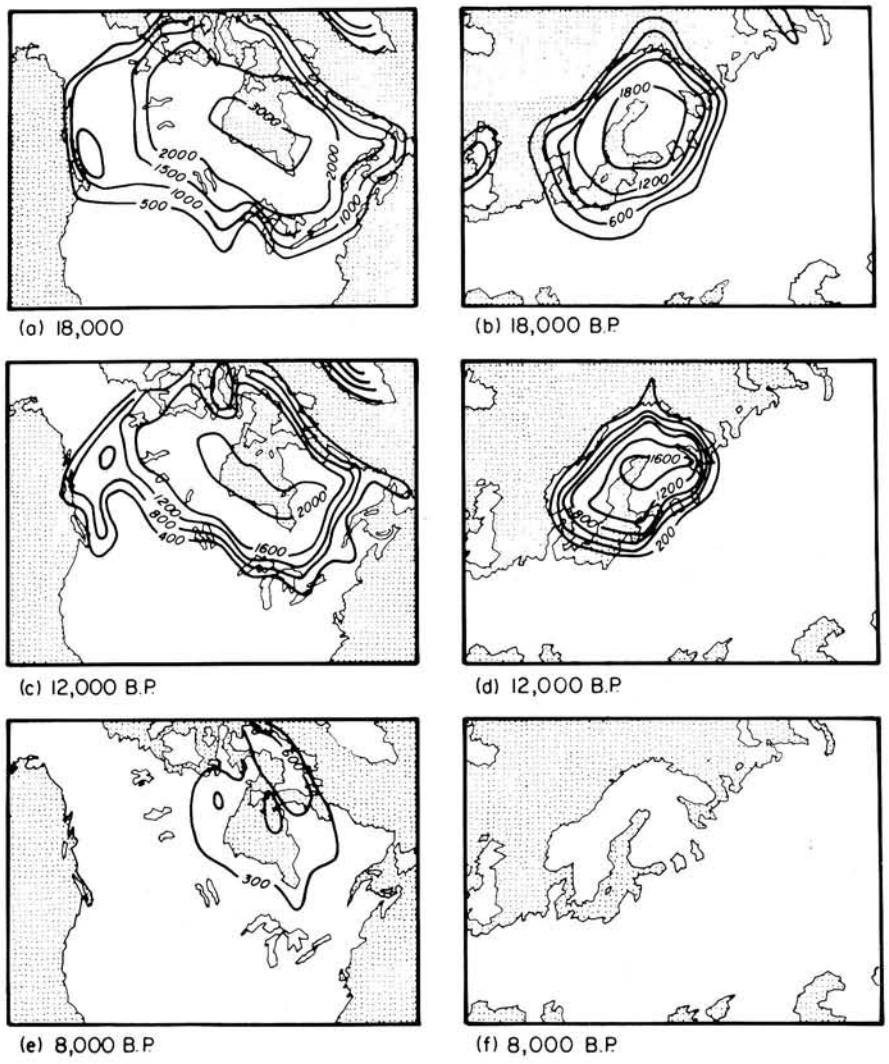

FIGURE 4.3 Time slices through the ICE-2 deglaciation chronology of Wu and Peltier (1983). Ice thickness is shown at three times for both the Laurentian and Fennoscandian ice sheets.

Figure 4.4, comparisons are shown for three different models that differ from one another only in terms of their lithospheric thicknesses. Inspection of these comparisons shows that the RSL data at sites inside the ice margin are reasonably well fit by the theoretical model and that the RSL variations at these sites are rather insensitive to changes of lithospheric thickness. This is entirely expected as the spatial scale of the Laurentian ice sheet (Figure 4.3) is so large that the lithosphere is transparent to the response at locations that were once under the ice-sheet center. At sites in the peripheral region, on the other hand, the response is extremely sensitive to lithospheric thickness as the deformation at such sites is significantly affected by relatively short horizontal wavelengths that see the lithosphere clearly. This sensitivity was first exploited (Peltier, 1984b) to measure lithospheric thickness, and a relatively high value in excess of 200 km was obtained. As reviewed in Peltier (1982), the totality of ^{14}C-controlled RSL data also requires an almost uniform profile of mantle viscosity with little variation between the upper and lower mantles. Weertman (1978) commented on this result from the point of view of theoretical ideas concerning the microphysical basis of solid-state creep in the Earth and suggested that it might be taken to imply that the relaxation of the lower mantle that occurs in postglacial rebound is controlled by transient creep rather than the steady-state creep, which is assumed in the Maxwell analogue. This possibility may be tested using the simple Burger's body rheology derived in Peltier *et al.* (1981), which includes the transient component of the response via a single Debye peak governed by two additional physical constants. An analysis of the asymptotic properties of the Burger's body rheology, however, demonstrates that when the elastic defect is large and the short- and long-time-scale viscosities sufficiently

different, the Burger body rheology again behaves like a Maxwell solid but with a viscosity equal to that which governs the short-time-scale transient response. Under these circumstances the lower mantle viscosity inferred by analysis of rebound data based on the Maxwell analogue would be the transient viscosity as originally suggested by Weertman (1978).

The Free-Air Gravity Anomaly over Centers of Post-Glacial Rebound

Figure 4.5 shows maps of the free-air gravity anomalies over the present-day centers of postglacial rebound in Canada [Figure 4.5(a)] and Fennoscandia [Figure 4.5(b)]. Comparison of these maps with those for ice thickness at glacial maximum, shown previously in Figure 4.3, demonstrates a high degree of correlation between these two fields and provides strong support for the hypothesis that the observed free-air anomalies are to be interpreted as measures of the currently existing degree of isostatic disequilibrium of these two regions. Figure 4.6 shows a comparison of observed and predicted present-day peak free-air anomalies for Laurentia and Fennoscandia for a number of Earth models having fixed lithospheric thickness of 120.7 km, and an upper mantle viscosity of 10^{21} Pa s as required by the sea-level data discussed previously. The Earth models employed differ from one another only in terms of their elastic structures, and lower mantle viscosity is varied through the same sequence of values for all models. As described in the figure caption, four of the

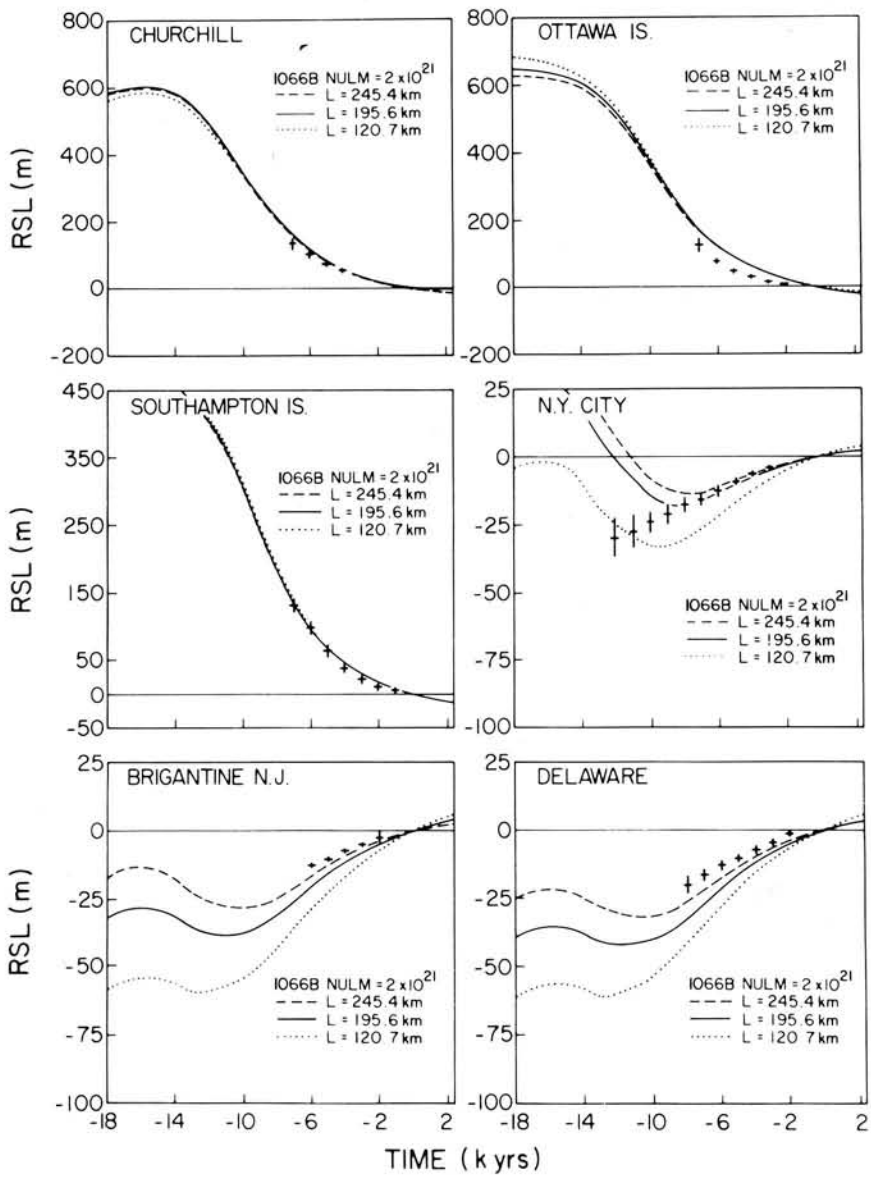

FIGURE 4.4 Observed RSL histories at 6 North American sites and predictions based on the ICE-2 melting chronology coupled with an Earth model having 1066B elastic structure, an upper-mantle viscosity of 10^{21} Pa s, and a lower-mantle viscosity of 2×10^{21} Pa s. Theoretical predictions are shown for models that differ only in their lithospheric thicknesses. The response is sensitive to this parameter only at the last three sites (d, e, and f), which are located in the peripheral bulge region south of the ice sheet margin along the U.S. east coast.

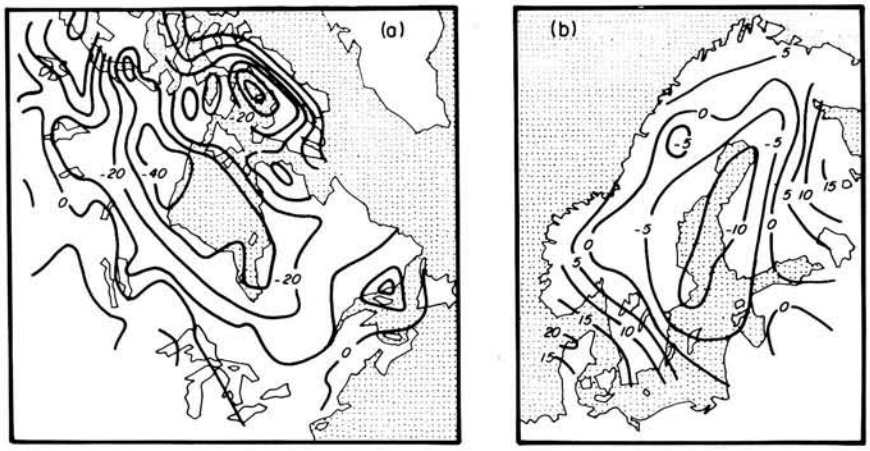

FIGURE 4.5 Observed free-air gravity anomalies over (a) Canada and (b) Fennoscandia. The locations of these anomalies should be compared with the ice-sheet topographic maxima shown on Figure 4.3.

models are flat, homogeneous, layered approximations to the 1066B elastic structure that have either one or two internal discontinuities of elastic parameters within the mantle at 420 km and/or 670 km depth corresponding to the depths to the olivine → spinel and spinel → post-spinel phase boundary horizons. The remaining two curves are for the seismically realistic models 1066B of Gilbert and Dziewonski (1975) and PREM of Dziewonski and Anderson (1981). In these models, all of the radial variation of density is treated as though it were nonadiabatic. Inspection of these results shows that fitting the observed free-air gravity anomalies with a model with weak radial

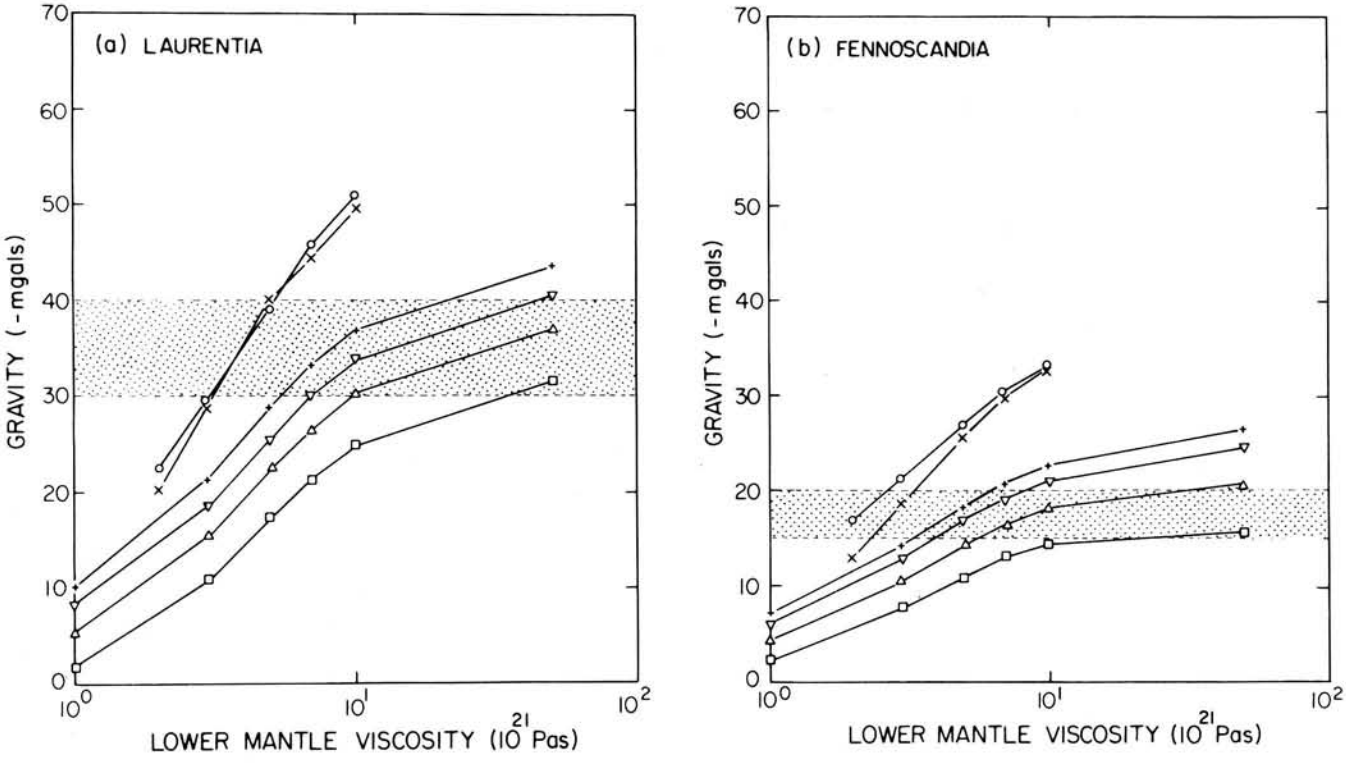

FIGURE 4.6 Observed (hatched regions) and predicted peak free-air gravity anomalies for both Laurentia and Fennoscandia. Predictions of the peak free-air anomaly are shown as a function of lower mantle viscosity with the upper mantle value held fixed at 10^{21} Pa s and the lithospheric thickness fixed at 120 km. The individual curves are predictions for models that differ only in their elastic structures: (×) 1066B; (○) PREM; (+) flat incompressible approximation to 1066B with a single internal density discontinuity with 12 percent increase at 670 km depth: (▽) same as (+) but having a 6 percent increase at 670 km depth and a 3 percent increase at 420 km depth; (△) same as (+) but having only a 6 percent increase of density at 670 km depth; and (□) same as (+) but having no internal density discontinuities in the mantle. See text for discussion.

variation of viscosity requires the presence in the model of significant internal buoyancy associated with a density structure that behaves nonadiabatically on the time scales of glacial rebound. This requires at least that the density variations across the phase boundaries at 420 and 670 km depth behave in this fashion, which is possible only to the extent that these transitions may be considered univariant (e.g., O'Connell, 1976; Mareschal and Gangi, 1977). Although such behavior is not inconceivable, it may also prove possible to reconcile these data by appealing to other physical effects. This is clearly an extremely important issue insofar as the problem of mantle convection is concerned (Peltier, 1985b). In any event, the demonstration that the incorporation of internal buoyancy of the mantle allows the essentially isoviscous model preferred by the sea-level data to simultaneously reconcile the large observed free-air anomalies does rather strongly undermine the claim of Walcott (1970, 1980) that these anomalies require that the viscosity of the lower mantle be high.

PLEISTOCENE DEGLACIATION AND EARTH ROTATION

From about 1900 until 1982 the location of the Earth's north pole of rotation was carefully monitored by the ILS using a global network of photo-zenith tubes equipped observatories. Since 1982 this observing system has been replaced by the much more accurate VLBI-based network of the IRIS Earth-orientation monitoring system that routinely determines the pole position at 5-day intervals with a verified accuracy of 2 milliseconds of arc (Carter and Robertson, 1985). Although these new data will quickly replace the old as the industry standard, the duration of the time series is still sufficiently short that the ILS data remain the best source of information on the secular motion of the pole. These data are shown in Figure 4.7 as x and y components of the displacement relative to the axes shown on the inset polar projection. The origin of the coordinate system corresponds to the Conventional International Origin (CIO). Inspection of these data, which are based on the reduction by Vincente and Yumi (1969, 1970), demonstrates that the dominant oscillatory signal, which consists of a 7-yr periodic beat generated by the interference between the 14-month Chandler and 12-month annual wobbles, is superimposed on a secular drift at the rate of $0.95° \pm 0.15°/10^6$ yr toward Hudson Bay. The direction of this drift is shown by the arrow on the inset polar projection of Figure 4.7.

In 1952, Munk and Revelle interpreted this observed secular drift of the rotation pole as requiring some present-day variation of surface mass load and suggested that the cause of the apparently required variation might be found in the melting of ice on Greenland and/or Antarctica. Their inference that such an effect was required to explain the data was, however, based on a dynamical model in which it was assumed that the Earth could be treated as a homogeneous viscoelastic sphere insofar as its rotational response to surface loading was concerned. To the extent that this approximation is valid, the inference of Munk and Revelle is completely correct since the theory then shows that the pole must be fixed at any instant of time in which the surface load is steady. As demonstrated by Peltier (1982), this holds true for homogeneous Earth models, since in this limit the isostatic adjustment and rotational contributions to the rotational forcing exactly annihilate one another. For radially stratified models, however, the dynamical symmetry that underlies this cancellation is broken and polar wander can occur even at a time when the surface load is steady. It therefore becomes plausible that the secular drift of the rotation pole shown on Figure 4.7 could simply be an effect due to the influence of planetary deglaciation that began 18 ka and ended about 7 ka. In Peltier (1982), Peltier and Wu (1983), Peltier (1984a), and Wu and Peltier (1984), it was in fact demonstrated that both the observed rate and direction of drift were just as expected if the Earth has the viscoelastic stratification required by the previously discussed RSL and free-air gravity data, and if the only forcing to which the system has been subject is that due to a glaciation-deglaciation cycle that ended about 7 ka.

Figure 4.8 illustrates the nature of the fit to the observed polar-wander speed as a function of the viscoelastic model employed to make the prediction. Observations of oxygen-isotope composition in deep-sea sedimentary cores (e.g., Peltier, 1982) are employed to constrain the cyclic variation of planetary ice cover that has occurred over the past 10^6 yr. These data demonstrate that the major continental ice masses have appeared and disappeared in a highly periodic fashion with a time interval of 10^5 yr separating successive interglacials. Individual glaciation pulses in the sequence are each observed to have a sawtooth form with a slow glaciation period lasting about 9×10^4 yr followed by a fast collapse lasting 10^4 yr. The calculations illustrated in Figure 4.8 are based on the assumption that seven such cycles have occurred and the observed polar-wander speed of about $1°/10^6$ yr is shown at a time 6000 yr following the last 10^4-yr disintegration event. Again this choice gives a best fit of the simple glaciation history model to the oxygen isotope data. Polar-wander speed predictions are shown on this figure for six different viscoelastic models of the interior, each of which has the same lithospheric thickness $\bar{L} = 120$ km. The prediction denoted by L0F (no core) is for the homogeneous model and verifies that the predicted speed following the end of the last glaciation phase of the load cycle is essentially identically zero in accord with the theory of Munk and Revelle (1952). However, as radial structure is added to the model, the symmetry that enforces the null response in

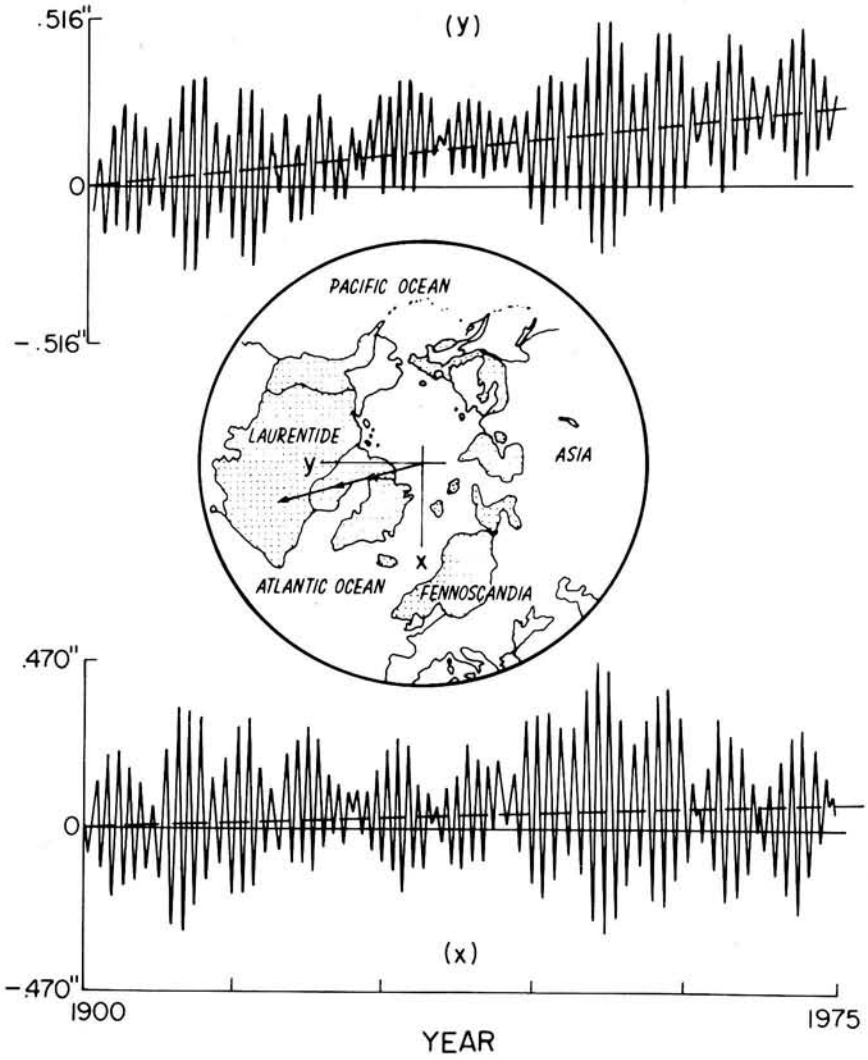

FIGURE 4.7 Position of the rotation pole relative to the CIO since 1900. See text for discussion.

the homogeneous model is broken, and the speeds predicted for times subsequent to the last glacial–deglacial pulse differ from zero. The effect of adding an inviscid high-density core to the model is illustrated by the calculation denoted L0F for which the elastic structure of the mantle is taken to be the average of model 1066B, and the mantle viscosity is assumed to have the value 10^{21} Pa s. Model L1F includes, in addition, the influence of the density jump at 670 km depth in the Earth based on the assumption that this discontinuity is capable of inducing a buoyant restoring force when it is displaced from equilibrium by the applied surface loads. The effect of this internal buoyancy in the mantle is to further increase the speed prediction in the model with 10^{21} Pa s uniform mantle viscosity. Adding a second density discontinuity at 420 km depth (model L2F with uniform viscosity) does not produce a significant further increase in the speed prediction, however. The final calculation illustrated on Figure 4.8, denoted L2F ($\nu_{LM} = 3 \times 10^{21}$ Pa s), demonstrates that the predicted speed can be reduced to the observed speed simply by elevating the viscosity of the lower mantle to the same value required by the free-air gravity and RSL data discussed previously. As discussed in Wu and Peltier (1984), this model also correctly predicts the observed direction of polar wander. These results establish that the data shown in Figure 4.7 cannot be construed as requiring any currently ongoing variation in surface load due to ice-sheet disintegration on Greenland and Antarctica. Rather, they are entirely explicable as a memory of the planet of the last deglaciation event of the current ice age, an event that was complete by about 7 ka.

A second effect of deglaciation on Earth's rotation addressed here concerns its influence on rotation rate and, therefore, on the so-called length of day (l.o.d.). Although the most important ongoing change in l.o.d. is the deceleration of the rate of rotation due to the gravitational

interaction between Earth and Moon through the agency of the lunar semidiurnal tide in the oceans, it has been known for some time that at least one other source of l.o.d. variation must exist. Analysis of ancient eclipse data (e.g., Müller and Stephenson, 1975) demonstrated that if one assumes that the lunar-tidal torque has been constant over the past few thousands of years and uses this assumption to predict the times and locations in the past of total eclipses of the Sun and Moon, then as one goes further back into the past, one makes an increasingly large systematic error in the predictions, which is such as to imply the action of a nontidal acceleration of rotation that is working in opposition to the tidal effect. Lambeck (1980) summarized such estimates and concluded that the best available from such data is the number $(\dot{\omega}/\omega)_{NT} = (6.9 \pm 2.6) \times 10^{-11}$/yr. A recent confirmation of this number has been provided through analysis of 5.5 yr of laser-ranging data to the LAGEOS satellite that has delivered an estimated of $(\dot{\omega}/\omega)_{NT} = (7.1 \pm 0.6) \times 10^{-11}$/yr (Yoder *et al.*, 1983). Peltier (1982, 1983) demonstrated that this observed rate of nontidal acceleration was also predicted as an effect of the last deglaciation event of the current ice age. In this analysis, exactly the same model as that employed to fit the secular drift of the pole revealed in the ILS data was employed to predict $(\dot{\omega}/\omega)_{NT}$, and the results are shown on Figure 4.9. The three calculations illustrated

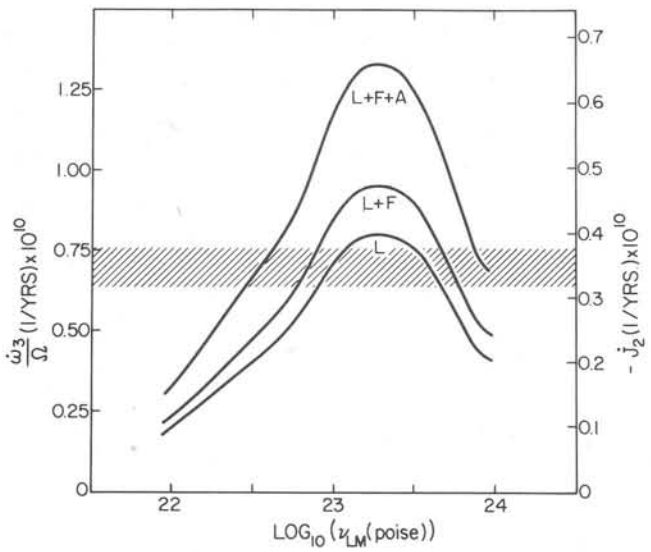

FIGURE 4.9 Observed nontidal acceleration of rotation, $(\dot{\omega}/\omega)_{NT}$, and equivalent $\dot{J}_2$ obtained from the analysis of laser-ranging data to the LAGEOS satellite. Predictions are shown as a function of lower mantle viscosity for models with 1066B elastic structure and for models that include only one ice sheet (L), two ice sheets (L + F), and three ice sheets (L + F + A). See text.

on this figure are for loading models that include only the Laurentian ice sheet (L), one that also includes the effect of the Fennoscandian ice sheet (L + F), and one that adds the effect of the West Antarctic ice sheet melting to that of the other two (L + F + A). The influence of the latter is clearly much more important as a source of forcing for rotation rate than as a source of forcing for polar wander. All speed predictions are shown as a function of lower mantle viscosity ν_{LM} with the upper mantle value held fixed at 10^{21} Pa s. Again, the preferred value of ν_{LM} is near 3×10^{21} Pa s. As mentioned previously, the lower-mantle viscosity could very well be associated with the transient component of the response rather than with the steady-state component that would govern the long-time scale thermal circulation. The manner in which the interpretations of both of these rotational data are influenced by small ice sheets and glaciers has been discussed in detail by Peltier (1988).

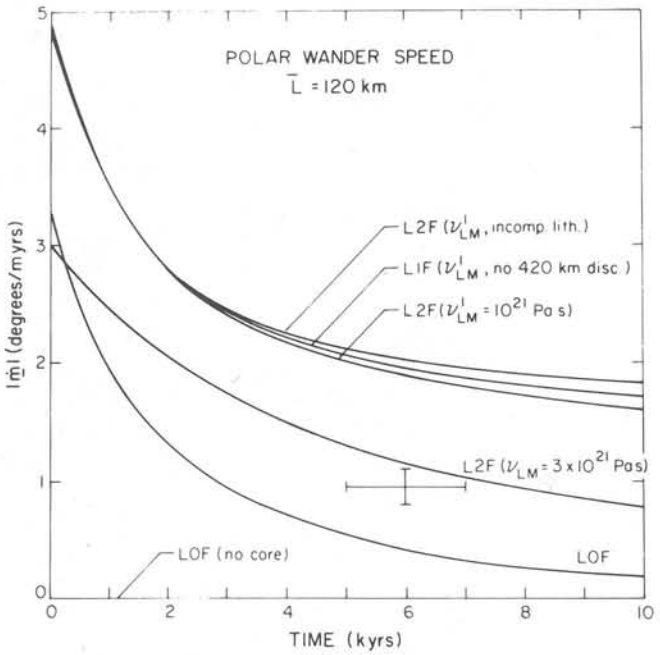

FIGURE 4.8 Predictions of polar-wander speed for several different viscoelastic models discussed in the text. The observed speed obtained from the secular rate of drift visible on Figure 4.7 is shown as the cross.

SECULAR VARIATIONS OF RELATIVE SEA LEVEL WITH GLACIAL ISOSTASY REMOVED

Given that the global model of glacial isostasy, described above, is able to explain much of the observed variability in the record of RSL change over the past 10^4 yr, it is natural to employ it to filter from the recent historical record of tide-gauge observations of secular sea-level change that component which is due to this cause.

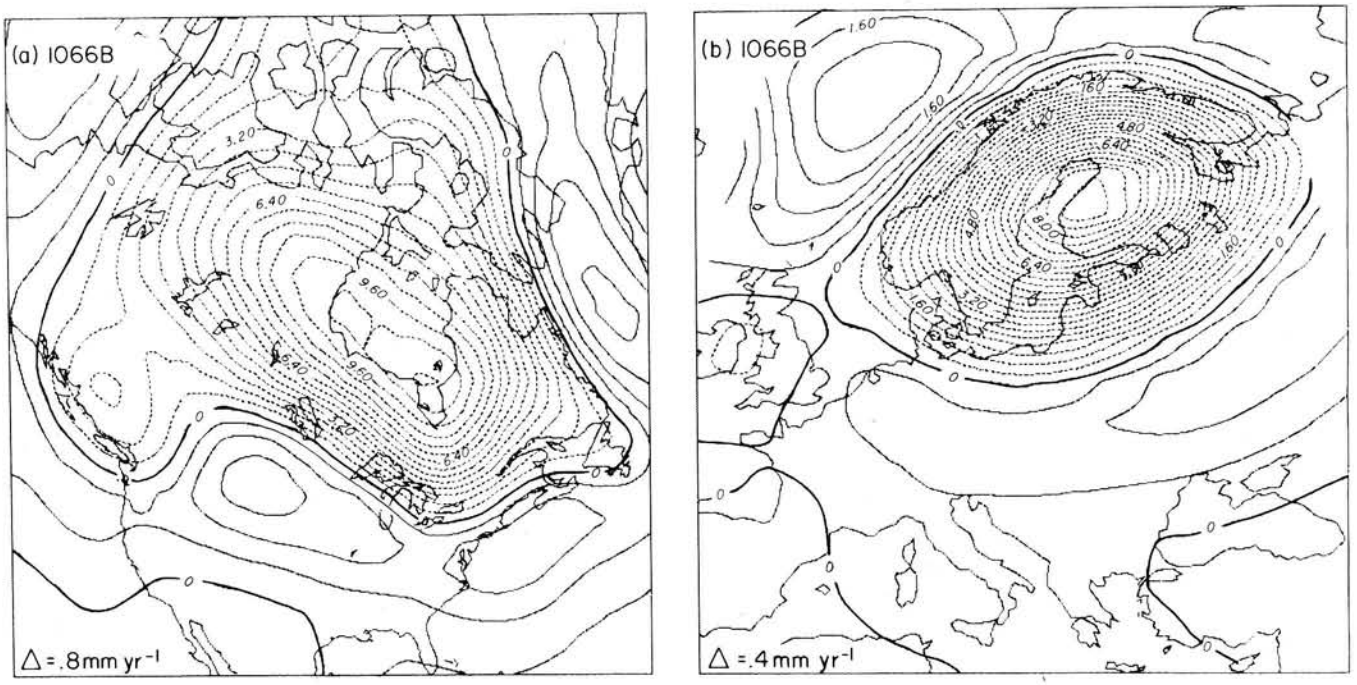

FIGURE 4.10 Continent scale maps of the predicted rate of vertical motion of the surface of the solid earth relative to the geoid using a "best" viscoelastic model with parameters fixed by fitting to the data of postglacial rebound and the ICE-2 deglaciation history shown on Figure 4.3: (a) is for North America and (b) for Europe. Dashed contours are in regions in which the land is currently rising out of the sea and solid contours are in regions that are currently submerging. Rates of vertical motion are in units of millimeters per year and the contour intervals are shown on the individual maps.

One simply employs the data in the long-time scale records of RSL history (controlled by ^{14}C dating) to constrain the viscous component of mantle rheology. One then employs this Earth structure to predict the present-day rate of sea-level rise and fall that should be observed at any location at which a tide gauge is installed, subtracts this prediction from the secular trend observed on the tide gauge, and analyzes the filtered data so produced.

As a preliminary to this procedure, it is useful to first illustrate the continent-scale variability of present-day RSL variation that is predicted by the isostatic adjustment model. Figure 4.10 shows the present-day rate of sea-level rise and fall predicted for North America and northwestern Europe using an Earth model with 1066B elastic structure. The viscous component of the model is one that has a lithospheric thickness of 200 km, an upper-mantle viscosity of 10^{21} Pa s, and a lower-mantle viscosity of 2×10^{21} Pa s. This model provides a reasonably good fit to the ^{14}C record of RSL rise along the U.S. east coast when employed in conjunction with the ICE-2 deglaciation history of Wu and Peltier (1983). The rates shown in the continental interior (where no ocean exists) represent the rates of separation between the surface of the solid earth and the geoid at such locations. (The geoid is an imaginary surface continued inland from the oceans, on which the gravitational potential has the same value as that obtained on the sea surface.) Notable on these maps is the fact, mentioned above, that the present-day maximum rates of RSL fall in the regions that were once ice covered are near 1 cm/yr. Surrounding each of the two main Northern Hemisphere centers of postglacial rebound, however, are ring-shaped regions in which RSL is predicted to be rising at rates that may be as high as 2 mm/yr, a maximum calculated along the passive continental margin of the U.S. east coast. The variation with position along the coast is fairly extreme, however, with very low calculated values obtaining both to the north and to the south of the maximum. Notable also on this map is the fact that the predicted rates of glacial isostatic submergence along the U.S. west coast are rather different from those on the east coast. The former region is much further distant from the main Laurentian ice mass and is also quite strongly influenced by the separate Cordilleran ice sheet that existed west of the Canadian Rocky Mountains. As a consequence of these effects, the predicted variations of the rate of present-day RSL change along this active continental margin are more complex.

Examination of Figure 4.10(b) illustrates a similar degree of complexity of the pattern of present-day RSL change predicted by the model for northwestern Europe. The maximum present-day rates of RSL fall near the center of

uplift in the Gulf of Bothnia are again near 1 cm/yr. Surrounding this central region of uplift is the region of peripheral submergence. Again the latter region is very strongly asymmetric with respect to the former, just as in North America, a consequence of the geometric complexity of the distribution of water and land. One important feature of these results is the fact that rates of present-day sea-level rise are predicted to be much lower along the coast of France, which extends to the southwest away from the center of uplift in Fennoscandia, than those along the east coast of the United States, which is similarly located with respect to the larger Laurentian ice mass.

Perhaps the most interesting aspect of the predictions discussed above of the rates of present-day RSL variation induced by the most recent deglaciation, is that they may be compared directly to tide-gauge observations of these rates at any point on the Earth's surface that may be of interest. Figure 4.11 summarizes the comparisons. The tide-gauge observations employed to construct this figure consist of the secular trends extracted from the individual time series of observations at each gauge over the time interval 1940 to 1980 as published in the recent catalogue of the National Ocean Service (1983). Figure 4.11(a) shows the results of the analysis for sites along the U.S. east coast. Each cross represents the secular trend at a specific gauge corrected for the secular trend expected from the influence of glacial isostatic adjustment. These corrected data are plotted as a function of the distance (in radians) of each gauge from the station at Key West, Florida, which is the southernmost station along the coast. The northernmost data point is for the gauge at Eastport, Maine. Also shown on this figure is the secular drift that has been subtracted from the raw data to make the correction for isostatic disequilibrium. This correction attains a maximum near 2 mm/yr about midway along the coast with very small rates obtaining at sites in Florida and Maine to the south and north of the maximum, respectively. To give some indication of the error in the model predicted rates, the predictions are shown not only for the present (18,000 yr after glacial maximum) but also for

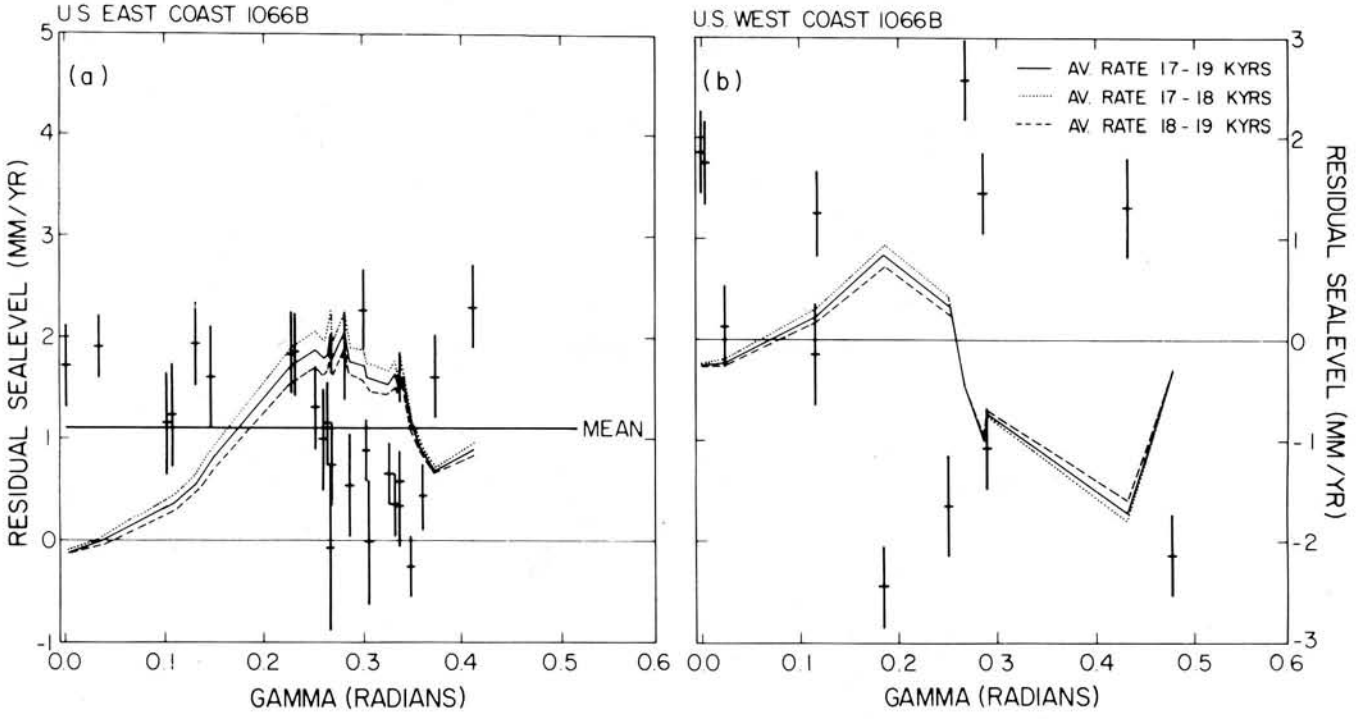

FIGURE 4.11 Tide-gauge secular trends of RSL rise along the (a) U.S. east coast and (b) west coast that have been corrected for the glacial isostatic motions shown on Figure 4.10 are shown as individual data points with the cross through the points indicating the error assigned to these data by the National Ocean Service (1983). The magnitude of the correction that was applied to the raw data is shown as a function of distance along each coast measured positive to the north of the southernmost tide gauge, which on the east coast is at Key West and on the west coast is at San Diego. Some indication of the error that might be involved in making the correction is provided by the three estimates of the isostatic rates computed at 500-yr separation through model "present." The solid line through the corrected data on (a) is the average secular rate of rise that remains after glacial isostatic contamination has been removed. No similar average was computed for the west coast data as the scatter is so extreme as to imply that the average would be meaningless physically.

17.5 ka and 18.5 ka. Noticeable on these predicted curves are the several locations at which the predicted rates deviate from the smooth variation of rate with distance that otherwise obtains. These are sites at which errors due to the finite-element discretization occur (see Wu and Peltier, 1983, for a detailed discussion of the finite-element discretization employed to solve the sea-level equation).

The main point to note by inspection of the data shown on Figure 4.11(a) is that the correction, due to the influence of glacial isostasy, of the secular rate of RSL rise along the U.S. east coast accounts for as much as 100 percent of the observed rate of rise at some sites. That is, at some sites along the U.S. east coast, all of the observed secular rates of rise are explicable in terms of the influence of glacial isostatic adjustment. In general, however, there is a systematic misfit between the predicted and the observed rates such that the observed rate of rise exceeds that predicted by the glacial isostatic adjustment model that fits the long-time scale, ^{14}C-controlled RSL histories. At no tide gauge along the U.S. east coast is the observed rate of rise significantly slower than that predicted by the adjustment model. The average of the reduced rates of RSL rise at sites in this region is also shown on Figure 4.11(a) and is near 1.1 mm/yr. The interpretation of this average in terms of a eustatic increase of sea level (either of steric or nonsteric origin) is clearly made rather difficult by virtue of the fact that the residual trends vary erratically as a function of distance along the coast. Other physical processes must be contributing substantially to the secular variations of RSL that individual gauges are recording.

An identical treatment of the tide-gauge data from the U.S. west coast is shown on Figure 4.11(b). Here, the corrected tide-gauge-observed rates of RSL rise are shown as a function of position, measured positive, north from the southernmost gauge, which in this case is the one located at San Diego. The observations along this active continental margin are much more erratically scattered than those along the passive east coast continental margin, demonstrating the severe contamination of this record (for our present purposes) that is presumably associated with local tectonic activity. Furthermore, the corrected data are scattered about zero and show no systematic bias toward positive rates as is evident for east coast sites. It would clearly be unreasonable to employ these data to make any inference whatsoever concerning eustatic sea-level variations.

CONCLUSIONS

The analysis of RSL variations presented in the previous sections of this chapter demonstrate that effects due to the most recent deglaciation of the current ice age continue in the modern record of sea-level change even though Würm-Wisconsin ice had disappeared from the continents by about 7 ka. In regions that were once ice covered, RSL is currently falling at a rate near 1 cm/yr due to this cause. In the immediately peripheral region of the collapsing forebulge, sea level would appear to be rising at rates in excess of 1 mm/yr due to the same process of glacial isostatic adjustment, if this were the only effect operative. The east coast of the continental United States is perhaps the best location illustrating this "drowning" effect, which is responsible for many of the unique features of its nearshore environment, including the extensive occurrence of salt marshes. A global model of glacial isostatic adjustment was described that has been employed to filter from the tide-gauge records of RSL change the influence of this effect. Although it is especially useful along the U.S. east coast, the model may also be applied to filter the global data base before these data are employed to draw conclusions concerning eustatic sea-level variations. An initial attempt to perform such a global analysis has been presented by Peltier and Tushingham (1989), whose analysis of all of the records in the data base (Permanent Service for Mean Sea Level, Bidston Observatory, Birkenhead, Mercyside, England) has led them to conclude that correcting the observed secular sea-level trends for the influence of glacial isostasy reveals a global eustatic signal with much increased coherence of strength of 2.4 ± 0.9 mm/yr. It is noteworthy that the secular drift of the rotation pole evident in the ILS pole path, which was previously interpreted by Munk and Revelle (1952) as requiring some ongoing decrease in surface ice load and thus a present-day increase in eustatic sea level, is also fully explicable as a rotational memory of the Earth of the most recent deglaciation of the current ice age, an event that ended about 7000 ka.

REFERENCES

Barnett, T. P. (1983). Possible changes in global sea level and their causes, *Climate Change 5*, 15–38.

Bloom, A. L. (1967). Pleistocene shorelines: A new test of isostasy, *Geol. Soc. Am. Bull. 78*, 1477–1493.

Carter, W. E., and D. S. Robertson (1985). Earth rotation from VLBI measurements, in *Space Geodesy and Geodynamics*, A. J. Anderson and A. Cazanave, eds., Academic Press.

Cathles, L. M. (1975). *The Viscosity of the Earth's Mantle*, Princeton University Press, Princeton, N.J.

Clark, J. A., W. E. Farrell, and W. R. Peltier (1978). Global changes in postglacial sea level: A numerical calculation, *Quat. Res. 9*, 265–287.

Dicke, R. H. (1969). Average acceleration of the Earth's rotation and the viscosity of the deep mantle, *J. Geophys. Res. 74*, 5895–5902.

Dziewonski, A. M., and D. L. Anderson (1981). Preliminary reference Earth model, *Phys. Earth Planet. Int. 25*, 297–356.

Farrell, W. E., and J. A. Clark (1976). On postglacial sea level, *Geophys. J. Roy. Astron. Soc. 46*, 647–667.

Gilbert, F., and A. M. Dziewonski (1975). An application of normal mode theory to the retrieval of structural parameters and source mechanisms from seismic spectra, *Phil. Trans. Roy. Soc. Ser. A*, 187–269.

Gornitz, V., L. Lebedeff, and J. Hansen (1982). Global sea level trend in the past century, *Science 215*, 1611–1614.

Hansen, J., D. Johnson, A. Lacis, S. Lebedeff, P. Lee, D. Reid, and G. Russell (1981). Climate impact of increasing atmospheric carbon dioxide, *Science 213*, 957–966.

Lambeck, K. (1980). *The Earth's Variable Rotation: Geophysical Causes and Consequences*, Cambridge University Press, Cambridge, England, 449 pp.

Mareschal, J.-C., and A. F. Gangi (1977). Equilibrium position of phase boundary under horizontally varying surface loads, *Geophys. J. Roy. Astron. Soc. 49*, 757–772.

Meier, M. F. (1984). Contribution of small glaciers to global sea level, *Science 226*, 1418–1421.

Müller, P. M., and F. R. Stephenson (1975). The acceleration of the Earth and Moon from early astronomical observations, in *Growth Rhythms and History of the Earth's Rotation*, G. D. Rosenberg and S. K. Runcorn, eds., John Wiley and Sons, New York, pp. 459–534.

Munk, W. H., and R. Revelle (1952). On the geophysical interpretation of irregularities in the rotation of the Earth, *Mon. Not. Roy. Astron. Soc. Geophys. Suppl. 6*, 331–347.

National Ocean Service (1983). *Sea-Level Variations for the United States 1855–1980*, U.S. Dept. of Commerce, National Oceanic and Atmospheric Administration, Rockville, Maryland.

O'Connell, R. J. (1971). Pleistocene glaciation and the viscosity of the lower mantle, *Geophys. J. Roy. Astron. Soc. 23*, 299–327.

O'Connell, R. J. (1976). The effects of mantle phase changes on postglacial rebound, *J. Geophys. Res. 81*, 971–974.

Peltier, W. R. (1974). The impulse response of a Maxwell Earth, *Rev. Geophys. Space Phys. 12*, 649–669.

Peltier, W. R. (1980). Mantle convection and viscosity, in *Physics of the Earth's Interior*, A. M. Dziewonski and E. Boschi, eds., North Holland, Amsterdam, pp. 362–431.

Peltier, W. R. (1981). Ice age geodynamics, *Ann. Rev. Earth Planet Sci. 9*, 199–225.

Peltier, W. R. (1982). Dynamics of the ice age Earth, *Adv. Geophys. 24*, 1–146.

Peltier, W. R. (1983). Constraint on deep mantle viscosity from LAGEOS acceleration data, *Nature 304*, 434–436.

Peltier, W. R. (1984a). The rheology of the planetary interior, *Rheology 28*, 665–697.

Peltier, W. R. (1984b). The thickness of the continental lithosphere, *J. Geophys. Res. 89*, 11303–11316.

Peltier, W. R. (1985a). The LAGEOS constraint on deep mantle viscosity: Results from a new normal mode method for the inversion of viscoelastic relaxation spectra, *J. Geophys. Res. 90*, 9411–9421.

Peltier, W. R. (1985b). Mantle convection and viscoelasticity, *Ann. Rev. Fluid Mech. 17*, 561–608.

Peltier, W. R. (1988). Global sea level rise and Earth rotation, *Science 240*, 895–901.

Peltier, W. R., and J. T. Andrews (1976). Glacial isostatic adjustment I: The forward problem, *Geophys. J. Roy. Astron. Soc. 46*, 605–646.

Peltier, W. R., and A. M. Tushingham (1989). Global sea level rise and the greenhouse effect: Might they be connected? *Science 244*, 806–810.

Peltier, W. R., and P. Wu (1982). Mantle phase transitions and the free air gravity anomalies over Fennoscandia and Laurentia, *Geophys. Res. Lett. 9*, 731–734.

Peltier, W. R., and P. Wu (1983). Continental lithospheric thickness and glaciation induced true polar wander, *Geophys. Res. Lett. 10*, 181–184.

Peltier, W. R., W. E. Farrell, and J. A. Clark (1978). Glacial isostasy and relative sea level: A global finite element model, *Tectonophysics 50*, 81–110.

Peltier, W. R., P. Wu, and D. A. Yuen (1981). The viscosities of the planetary mantle, in *Anelasticity in the Earth*, F. D. Stacey, A. Nicholas, and M. S. Paterson, eds., American Geophysical Union, Washington, D.C.

Russell, R. J., ed., (1961). Pacific Island Terraces: Eustatic? *Zeit. Geomorph. Suppl. 3*, 106 pp.

Sabadini, R., and W. R. Peltier (1981). Pleistocene deglaciation and the Earth's rotation: Implications for mantle viscosity, *Geophys. J. Roy. Astron. Soc. 66*, 552–578.

Vincente, R. O., and S. Yumi (1969, 1970). Co-ordinates of the pole (1899–1968), returned to the conventional international origin, *Publ. Int. Latitude Observ. Mizusawa 7*, 41–50.

Walcott, R. I. (1970). Isostatic response to loading of the crust in Canada, *Can. J. Earth Sci. 7*, 716–727.

Walcott, R. I. (1980). Rheological models and observations of glacio-isostatic rebound, in *Earth Rheology, Isostasy and Eustasy*, N.-A. Mörner, ed., John Wiley and Sons, New York, pp. 3–10.

Weertman, J. (1978). Creep laws for the mantle of the Earth, *Phil. Trans. Roy. Soc. London A288*, 9–26.

Wu, P., and W. R. Peltier (1983). Glacial isostatic adjustment and the free–air gravity anomaly as a constraint on deep mantle viscosity, *Geophys. J. Roy. Astron. Soc. 74*, 377–449.

Wu, P., and W. R. Peltier (1984). Pleistocene deglaciation and the Earth's rotation: A new analysis, *Geophys. J. Roy. Astron. Soc. 76*, 753–792.

Yoder, C. F., J. G. Williams, J. O. Dickey, B. E. Schutz, R. J. Eanes, and B. D. Tapley (1983). J_2 from LAGEOS and the nontidal acceleration of Earth rotation, *Nature 303*, 757–762.